

Absolute L-shell ionization and X-ray production cross sections of Lead and Thorium by 16-45 keV electron impact

H. V. Rahangdale,^{*} P. K. Das,[†] S. De,[†] J. P. Santos,[‡] D. Mitra,[§] M. Guerra,[¶] and S. Saha[†]

The absolute L subshell specific electron impact ionization cross sections near the ionization threshold ($16 < E < 45$ keV) of Lead and Thorium are obtained from the measured L X-ray production cross sections. Monte Carlo simulation is done to account for the effect of the backscattered electrons, and the final experimental results are compared with calculations performed using distorted wave Born approximation and the modified relativistic binary encounter Bethe model. The sensitivity of the results on the atomic parameters is explored. Observed agreements and discrepancies between the experimental results and theoretical estimates, and their dependence on the *specific* atomic parameters are reported.

I. INTRODUCTION

Importance of electron impact excitation and ionization data in various materials analysis techniques such as electron probe microanalysis (EPMA), Auger electron spectroscopy (AES), etc. need not be overemphasized. Precise and accurate knowledge of the corresponding cross sections is used as input either in the form of look-up tables or functional dependence on electron impact energies of the electron probe used for such analysis. The inner shell ionization probabilities, extracted from the above-mentioned data, are also pivotal to many other material analysis techniques, apart from their importance in understanding the physical process of ionization in multi-electron bound systems [1].

Inner shells of atoms can be excited by knocking off the bound electrons to the continuum or unfilled quasi-bound orbitals. Vacancies thus created are filled by the electrons from the outer shells, resulting in the emission of photons. In addition, migration of vacancies through Coster-Kronig (CK) transitions among different subshells (L -shell and above) as well as to other inner shells, leads to photon emission with different energies and yields, which are complicated by the fact that the corresponding transition probabilities need to be accurately known. From the observation and quantitative estimation of the related photon yield with high precision, the inner shell ionization cross sections can be obtained, in principle, utilizing the known or pre-determined parameters, such

as the fluorescence yield, CK transition probabilities and the sublevel-specific radiative decay probabilities from experiments or theoretical estimates. These important parameters are collectively known as the atomic relaxation parameters.

The above mentioned relaxation parameters are obtained from experiments or from theoretical estimates [2] and are available from various data bases. However, some of these parameters are quoted with large uncertainties due to various processes involved. For example, the fluorescence yield for a specific subshell depends on the primary vacancy distributions, which in turn depends on the mode of vacancy creation in the subshell. It is also expected that migration of vacancies through CK transition would alter the primary vacancy distributions and hence the fluorescence yield.

Photon emission by electron impact is also possible as a multistep process through Auger transition, followed by creation of vacancy in the inner subshells by virtual photons [3]. The above process involving virtual photons can only be accounted for by invoking quantum electrodynamics and the associated electromagnetic interaction between the bound electrons, which involve both Coulomb interaction and the magnetic interaction due to the moving electrons. In case of lighter elements, the motion of inner shell electrons are in the non-relativistic regime ($v/c \rightarrow 0$), and therefore, the quantum effects due to magnetic interaction becomes negligible. Thus, inclusion of the Coulomb interaction alone in estimating the electron impact ionization cross sections results in reasonable agreement with the experimental results for the lighter atoms. For heavier atoms like the ones considered in this experiment, the magnetic interaction can no longer be ignored, and related estimates of the electron impact ionization cross sections should take magnetic interaction into account as well. Theoretical estimates based on above has been done in recent times for Gold (Au) [4].

Experiments on electron impact ionization which were done earlier, were focused primarily on K -shell ionization cross section, while L and M shell ionization data were seldom reported [5]. One of the major problems faced in the interpretation of experimental results based on established theories is that the extracted subshell specific

^{*} hitesh.rahangdale@saha.ac.in; Applied Nuclear Physics Division, Saha Institute of Nuclear Physics, 1/AF, Bidhannagar, Kolkata-700064, India

[†] Applied Nuclear Physics Division, Saha Institute of Nuclear Physics, 1/AF, Bidhannagar, Kolkata-700064, India

[‡] Laboratório de Instrumentação, Engenharia Biomédica e Física da Radiação (LIBPhys-UNL), Departamento de Física, Faculdade de Ciências e Tecnologia, FCT, Universidade Nova de Lisboa, 2829-516 Caparica, Portugal

[§] Department of Physics, University of Kalyani, Kalyani, Nadia-741235, India

[¶] Centro de Física Atómica, CFA, Departamento de Física, Faculdade de Ciências e Tecnologia, FCT, Universidade Nova de Lisboa, 2829-516 Caparica, Portugal

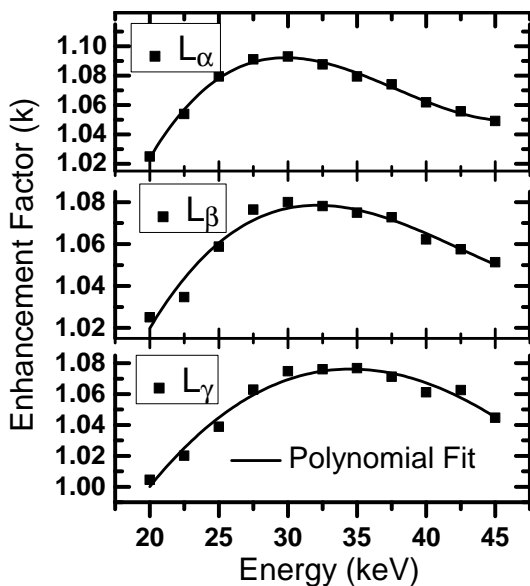


FIG. 1. Enhancement factor due to the presence of Aluminum backing in Thorium target, as obtained from PENELOPE simulation

ionization cross sections do not agree with the theoretical estimates for all the subshells. Recently, many authors have reported L X-ray production cross sections for a few elements, and validation of various theoretical models are done using the data. Comparison between theory and experimental data on L -subshell production cross sections in Gadolinium (Gd, $Z = 64$) and Tungsten (W, $Z = 74$) were done by Wu et al.[6]. Their experimental results on L_α and L_β lines agree reasonably well with DWBA theory including exchange interaction for W but deviates by 15-20% in case of Gd. Similar comparative studies were done by Varea et. al [7] on Hf, Ta, Re, Os, Au, Pb, and Bi, where experimental results for L_α and L_β lines are explained well by DWBA theory for Ta, Os, Au, Pb and Bi but are lower than the theoretical estimates by $\sim 35\%$ for Hf and Re.

In the present work, the $L_\alpha, L_\beta, L_\gamma$ production cross sections in Lead and Thorium are measured, and the results are converted to the subshell specific ionization cross sections. Because of the finite thickness of the target materials, single collision condition within the target has to be ensured. In arriving at the ionization cross sections from the production cross sections, corrections due to multiple collisions per beam traverse was done using a Monte Carlo simulation procedure. Parameter dependence in extracting the ionization cross sections are also explored to check the sensitivity to parameter variations. The cross sections obtained from experiment are compared with a) the theoretical results based on the distorted wave Born approximation (DWBA) including relativistic effects and exchange interactions into account [8], as obtained from the PENELOPE[9] code, and b) the modified relativistic binary encounter Bethe (MR-

BEB) [10, 11] model-based estimates. To the best of our knowledge, the subshell specific ionization cross section for all the L -subshells of Thorium are reported here for the first time at the energy values near the corresponding ionization threshold.

II. EXPERIMENTAL DETAILS

The Experimental set-up consists of an in-vacuum energy dispersive spectrometer with a focusable electron gun (up to 50 keV), electrically cooled silicon PIN diode based X-ray detector, thin film target holder, and Faraday cup. The X-ray detector was placed in the meridian plane at 55° with respect to the beam axis. The pressure maintained inside the vacuum chamber was 5×10^{-7} mbar. Details of the experimental arrangement are described elsewhere in detail[12].

The targets used in the experiment were made by using two different techniques. Self-supporting Lead targets were made by electron beam vapor deposition. The thickness of the thin film of Lead, deposited on a glass substrate was monitored during deposition using a quartz thickness monitor. Thorium targets were made by electro-deposition on $200 \mu\text{g}/\text{cm}^2$ thick Aluminum foil (99.99 % purity). Electro-deposition of Thorium oxide (ThO_2) on the foil cathode from a Thorium nitrate solution in 2-propanol solvent, was monitored by measuring the electrode current and the duration of deposition. Foil thicknesses were measured by an alpha energy loss spectrometer[12] and the measured thicknesses are $78.1 \pm 3.8 \mu\text{g}/\text{cm}^2$ (Th) and $82.0 \pm 4.2 \mu\text{g}/\text{cm}^2$ (Pb).

X-rays generated due to electron impact were detected by X-ray detector (model XR-100CR from Amptek, USA), having energy resolution of 165 eV (FWHM) for 5.9 keV photons. Mylar foil of $100 \mu\text{m}$ thickness was placed in front of the $25.4 \mu\text{m}$ Beryllium window to reduce flux of M X-rays. The efficiency of the detector was measured by (i) K -shell ionization of Copper by electron impact and (ii) using characteristic X-ray lines from a calibrated ^{241}Am source. The efficiency curve was fitted with equation $\epsilon(E) = 1.58 \times 10^{-5} + 1.31 \times 10^{-6}E - 8.63 \times 10^{-8}E^2$. The signal from the detector was fed to a multi-channel analyzer (MCA) through a shaping amplifier. For each data acquisition run, the count rates were kept low (< 300 counts/sec), so that there was no pile-up in the detector and therefore, no dead time correction was required for the MCA.

In the case of targets backed by the thick substrate, the electrons can be back-scattered from the substrate material and re-enter the target. These backscattered electrons can significantly change the original X-ray yield. It is necessary to correct for this enhancement of X-ray yield for the thick film backed targets like the Thorium targets used in this work. Also for obtaining the accurate ionization cross sections, one has to ensure that the target thickness is such that the projectile electrons do not ionize the target atoms more than once, thereby satisfying

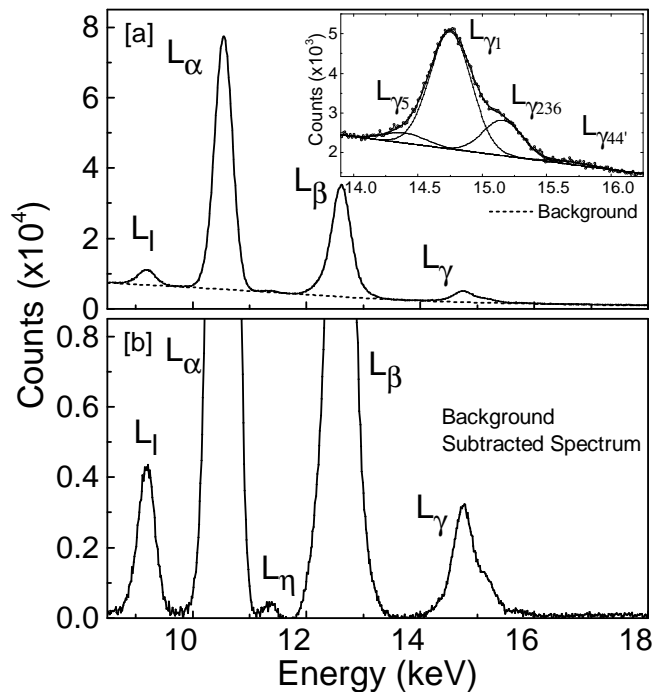


FIG. 2. Spectrum of Lead due to 35 keV electron impact. [a] Raw Spectrum with fitted L_{γ} are shown in the inset. [b] Same spectrum after background subtraction.

the single collision condition. A Monte Carlo simulation based on PENELOPE[9] computer code was performed to quantify the effect of electron back-scattering on the measured X-ray yield and thereby, ensure the inclusion of single collision events.

The Monte Carlo simulation code PENELOPE is a versatile program for estimation of the effects of electron-photon transport in materials. The main advantage of invoking a Monte Carlo simulation at this stage is: 1) ease of incorporating sophisticated interaction models and 2) convenience and capability of including arbitrary geometry into the calculation. However, in achieving this level of sophistication, the crystalline structure of the solid materials are completely ignored by considering the interacting media as homogeneous, isotropic and amorphous with definite composition and density. It is evident that such a *gas-like* model of the medium may be considered as a valid approximation for electron beam interaction with thin films of solids, however, the simulation results are likely to deviate from reality for thicker solid interaction media.

PENELOPE uses the combination of numerical and analytical physical interaction models to track down the encounter of electrons and photons with matter. Specifically, the effect of electron impact inner shell ionization is taken into account from the numerical differential cross sections (DCS)[13] obtained from DWBA based calculations[8].

While generating simulated X-ray spectra by PENE-

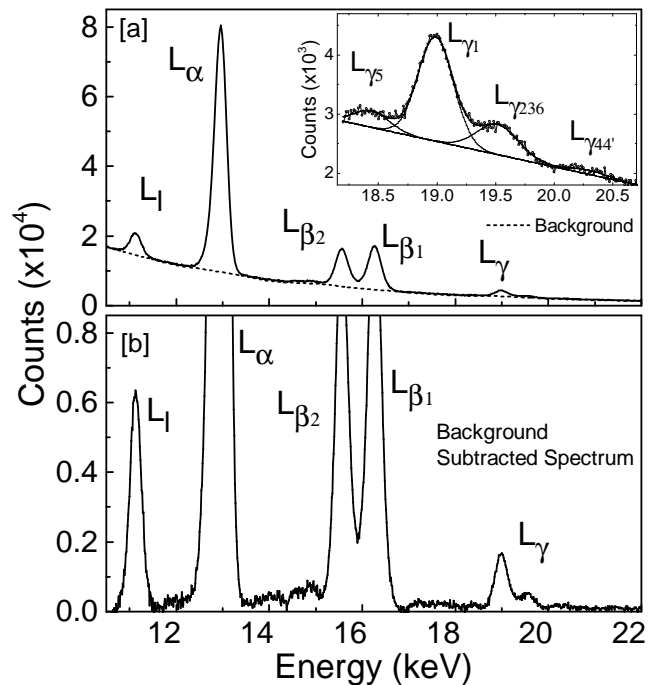


FIG. 3. Spectrum of Thorium due to 35 keV electron impact. [a] Raw Spectrum with fitted L_{γ} are shown in the inset. [b] Same spectrum after background subtraction.

LOPE, the process becomes inefficient and time consuming due to 1) low inner shell ionization and subsequent radiative decay probabilities, and 2) use of thin film media in the experiment. This results in large variance and reduces the predictive power of simulation. To reduce the time spent on computation and to increase the efficiency, it is necessary to use a variance reduction technique, known as interaction forcing. PENELOPE implements the process by artificially reducing the mean free path relevant to the process, but keeping the probability distribution functions for energy loss and angular deflections the same as for the real process. Finally, the biasing introduced by the simulation process is corrected for by applying appropriate statistical weights[9].

Simulation was carried out with a pencil-like electron beam of 2 mm diameter impinging on a thin target at normal incidence. Entry of the projectile electrons into the target, resulting ionization events and emission of X-rays were recorded event by event. From the simulation of a large sample of events, the maximum probability of inner shell ionization per projectile electron was ~ 0.53 for both the target films used in the experiment. This number, being less than unity, ensures that single collision condition was satisfied in the experiment.

To account for the effect of electron back-scattering in the Thorium target, simulation was done with and without aluminum backing. It was found that up to $\sim 4\%$ of the electrons which ionized the Thorium atoms and subsequently generated L X-rays were back-scattered

from aluminum. The back-scatter fraction, however, was found to depend on electron energy (E). After obtaining X-ray yield with good statistics from simulation, the corresponding enhancement factor $k(E)$ was obtained as:

$$k(E) = \frac{\text{Counts under } L_x \text{ peak for Al backed target}}{\text{Counts under } L_x \text{ peak for unbacked target}}, \quad (1)$$

where x is α , β or γ .

The $k(E)$ -values, obtained from simulation, are plotted in the Fig. 1 for the L X-rays. The values of $k(E)$ lies in the range: 1.005 to 1.095.

III. DATA ANALYSIS

The X-ray spectra of Lead and Thorium, resulting from electron bombardment at 35 keV, are shown in the Figs. 2 and 3 respectively. Individual L_x peaks in the observed spectra were fitted with Gaussian profile over the bremsstrahlung background, as shown in the figures, to obtain the corresponding X-ray yield (N_X). The bremsstrahlung background over the region of interest was considered as linear due to small interval of energy spanned by each peak. L_l and L_α peaks were fitted with single Gaussian functions for both Lead and Thorium. L_β peaks in Thorium could be resolved in $L_{\beta 1}$ and $L_{\beta 2}$, and were fitted with two Gaussian profiles. The L_β peaks could not be resolved for Lead and therefore, a single Gaussian with higher FWHM value was fitted. L_γ peaks in both the targets were resolved into three constituent lines viz., $L_{\gamma 5}$, $L_{\gamma 1}$, and $L_{\gamma 236}$. Fitted L_γ spectra are shown in the insets of Figs 2(a) and 3(a). The net counts obtained by fitting the spectra were corrected for self-absorption due to finite target thicknesses, assuming the oblique path of the X-rays through the target materials.

The X-ray production cross sections were obtained from the measurements using the formula:

$$\sigma_i(E) = \frac{N_X A}{\epsilon(E') t N_e N_A k(E)}, \quad (2)$$

where, $\sigma_i(E)$ is the production cross section of L_x line at projectile electron energy E , N_X is the net yield of X-rays after self-absorption correction during a time interval T , $\epsilon(E')$ is the effective efficiency of detector at photon energy E' which is the energy of L_x line centroid, t is the thickness of target, A is the mass number of the target material, N_e is the total number of electrons impinging on the target during the same interval T , N_A is the Avogadro number and $k(E)$ is the enhancement factor defined as above ($k = 1$ for Lead). The effective efficiency of the detector includes the effect of the geometric factor, attenuation due to Mylar and the intrinsic efficiency of the detector.

The experimentally obtained production cross sections were converted to the ionization cross sections using

Eqs. 3, 4, 5, given as:

$$\sigma_{L_1} = \frac{\sigma_{L_{\gamma 2+3}}}{\omega_1 S_{\gamma 2+3,1}}, \quad (3)$$

$$\sigma_{L_2} = \frac{\sigma_{L_{\gamma 1+5}}}{\omega_2 S_{\gamma 1+5,2}} - \sigma_{L_1} f_{12}, \quad (4)$$

$$\sigma_{L_3} = \frac{\sigma_{L_\alpha}}{\omega_3 S_{\alpha,3}} - \sigma_{L_1} (f_{12} f_{23} + f_{13}) - \sigma_{L_2} f_{23}. \quad (5)$$

$S_{i,I}$ is the fraction of radiative transition resulting from vacancy created in the I^{th} subshell associated with the L_i peak, ω_i is the fluorescence yields corresponding to subshells L_i , and f_{ij} is the Coster-Kronig transition probability between the L_i and L_j subshells. The production cross sections corresponding to the $L_{\gamma 1}$, $L_{\gamma 236}$ and L_α transitions are used in the above equations, which is the recommended combination (see ref. [14]), among many other combinations, to find the ionization cross sections. The atomic relaxation parameters, used in the calculations, are taken from the Refs. [15] and [16]. Tables I and II enlist all the parameters used in this work.

Target	ω_1	ω_2	ω_3	f_{12}	f_{13}	f_{23}
Lead	0.1	0.397	0.343	0.064	0.61	0.119
Thorium	0.17	0.503	0.424	0.06	0.66	0.103

TABLE I. Fluorescence yield and Coster-Kronig transition probabilities used in this work.

It is evident from Eq. 4 that the $L_{\gamma 2+3}$ production cross section is needed to obtain the L_1 sub-shell ionization cross section. However, it is not directly available from experiment due to the limited resolution of the X-ray detector. As mentioned earlier, the L_γ peak is resolved into $L_{\gamma 5}$, $L_{\gamma 1}$, and $L_{\gamma 236}$ lines. Therefore, the production cross section of $L_{\gamma 2+3}$ line is obtained by subtracting the contribution of $L_{\gamma 6}$ from the experimentally obtained $L_{\gamma 236}$ peak. The contribution of $L_{\gamma 6}$, in turn, is obtained from the ratio: $\Gamma_{\gamma 6}/\Gamma_{\gamma 1}$ and the $L_{\gamma 1}$ peak counts of the fitted spectrum.

The L_γ peaks were not observed at 16 keV electron impact energy for Lead, and at 20 and 22.5 keV energy for Thorium. Also at 25 keV electron beam energy, only $L_{\gamma 1}$ could be observed for Thorium and therefore, only the L_2 and L_3 ionization cross sections could be obtained. L_1 , L_2 and L_3 ionization cross sections were extracted from the data at all energies above 16 keV for Lead and 25 keV for Thorium.

The L_β line of Thorium was resolved into $L_{\beta 1}$ and $L_{\beta 2}$ peaks in the obtained spectra. To cross-check and verify the obtained ionization cross sections, attempts were made to extract the L_1 and L_2 ionization cross sections from the $L_{\beta 1}$ and $L_{\beta 2}$ production cross sections using the equations 6 and 7 [17].

Line	Source shell	Vacant shell	Transition Energy (keV)	Radiative Yield		Transition Energy (keV)	Radiative Yield	
				Yield (Γ)	Fraction ($S_{i,I}$)		Yield (Γ)	Fraction ($S_{i,I}$)
				Lead		Thorium		
l_i	M1	L3	9.184	0.085	0.0406	11.119	0.146	0.0449
l_{α_2}	M4	L3	10.449	0.164	0.0786	12.81	0.250	0.0765
l_η	M1	L2	11.347	0.052	0.0216	14.507	0.084	0.0215
l_{β_6}	N1	L3	12.141	0.021	0.0101	14.973	0.037	0.0115
l_{β_2}	N5	L3	12.623	0.293	0.1402	15.621	0.474	0.1451
l_{β_4}	M2	L1	12.304	0.456	0.3458	15.64	0.756	0.3588
l_{β_1}	M4	L2	12.614	1.884	0.7808	16.202	2.951	0.7598
$l_{\beta_{15}}$	N4	L3	12.601	0.032	0.0155	15.588	0.051	0.0158
l_{β_5}	O4	L3	13.013	0.042	0.0204	16.211	0.099	0.0305
l_{β_5}	O5	L3	13.013	0.042	0.0204	16.211	0.099	0.0305
l_{β_3}	M3	L1	12.791	0.501	0.3796	16.423	0.696	0.3303
l_{γ_5}	N1	L2	14.305	0.013	0.0056	18.361	0.022	0.0058
l_{γ_1}	N4	L2	14.762	0.404	0.1677	18.982	0.685	0.1765
l_{γ_2}	N2	L1	15.099	0.120	0.0909	19.302	0.207	0.0983
l_{γ_3}	N3	L1	15.215	0.145	0.1103	19.503	0.218	0.1036
l_{γ_6}	O4	L2	15.176	0.054	0.0227	19.596	0.133	0.0343
l_{γ_4}	O3	L1	15.775	0.052	0.0396	20.289	0.101	0.0478
l'_{γ_4}	O2	L1	15.755	0.052	0.0396	20.289	0.101	0.0478

TABLE II. Radiative yields for Lead and Thorium, from Campbell and Wang[16].

$$\begin{aligned} \sigma_{(L_{\beta_1}+L_{\beta_5}+L_{\beta_3})} &= S_{\beta_5,3}\omega_3\sigma_{L_3} + [S_{\beta_1,2}\omega_2 + S_{\beta_5,3}\omega_3 f_{23}] \sigma_{L_2} \\ &\quad + [S_{\beta_1,2}f_{12}\omega_2 + S_{\beta_5,3}\omega_3(f_{13} + f_{12}f_{23}) + S_{\beta_3,1}\omega_1] \sigma_{L_1}, \end{aligned} \quad (6)$$

$$\begin{aligned} \sigma_{(L_{\beta_2}+L_{\beta_6}+L_{\beta_4})} &= S_{\beta_2+6,3}\omega_3\sigma_{L_3} + S_{\beta_2+6,3}\omega_3 f_{23}\sigma_{L_2} \\ &\quad + [S_{\beta_2+6,3}\omega_3(f_{13} + f_{12}f_{23}) + S_{\beta_4,1}\omega_1] \sigma_{L_1} \end{aligned} \quad (7)$$

where, the symbols used have the usual meaning, as explained for equations (3, 4 and 5). The same set of atomic relaxation parameters was used. Ionization cross sections for L_3 subshell, needed as input, were obtained from the DWBA estimates. A good reason for using the theoretical estimates for L_3 subshell is that the experimental results are found to be in reasonable agreement (see Fig. 7).

The L_2 subshell ionization cross sections, obtained as above for the given energy range, were found to be in good agreement with the results obtained from the L_α and L_γ cross sections (see Eqs. 3, 4 and 5). However, the calculated σ_{L_1} values were not at all consistent with the corresponding results. Minor changes in the relaxation parameters within the allowed range of variation (see Ref. [15]) restores σ_{L_1} values to come closer to the previously obtained results (see Fig. 7), without causing much deviation in σ_{L_2} values. This indicates the need for possible modification of the atomic relaxation parameters.

IV. RESULTS AND DISCUSSION

The X-ray production cross sections, determined from the experiment and the ionization cross sections, obtained from the experimental data, are shown in Tables III and IV for Lead and Thorium respectively. The uncertainties in the cross section values are indicated. Overall uncertainties for L X-rays production cross sections are $\sim 11 - 12\%$ for both the elements. Contribution to the uncertainties are from 1) detector efficiency ($\sim 10\%$), 2) target thickness measurement ($\sim 5\%$) and 3) beam current measurement ($\sim 3\%$). Considering propagation of errors as per Eqs. (3, 4, 5), the uncertainties in the corresponding ionization cross sections are $\sim 20\%$, and including the uncertainties in the relaxation parameters within their quoted ranges, the errors in the ionization cross sections are larger $\sim 30\%$.

The experimental results are compared with the two different theoretical estimates based on two different formalisms: 1) MRBEB theory and 2) DWBA formalism. The DWBA theory based analytical formulas for calcu-

Energy (KeV)	Production cross section			Ionization cross section		
	L_α (barn)	L_β (barn)	L_γ (barn)	L_1 (barn)	L_2 (barn)	L_3 (barn)
16	43.5(5.2)	9.9(1.2)	164.5(20.6)
18	55.3(6.7)	21.7(2.6)	1.4(0.2)	3.9(2.2)	21.9(4.0)	204.4(26.3)
20	117.7(14.2)	52.6(6.4)	4.5(0.5)	22.8(8.7)	64.6(11.6)	423.7(56.1)
23	129.1(15.6)	63.2(7.6)	6.1(0.7)	44.6(14.7)	84.0(15.4)	451.0(62.0)
25	137.3(16.6)	70.1(8.5)	6.8(0.8)	49.7(16.4)	93.7(17.2)	477.6(66.0)
28	146.6(17.7)	76.8(9.3)	8.3(1.0)	63.4(20.6)	113.4(20.7)	502.0(70.8)
30	159.0(19.2)	83.8(10.1)	8.9(1.1)	72.3(23.1)	119.9(22.1)	542.6(76.8)
33	154.3(18.6)	84.8(10.2)	9.0(1.1)	76.1(23.9)	119.8(22.1)	522.6(74.7)
35	154.0(18.1)	90.2(10.9)	9.0(1.1)	70.4(22.6)	121.7(22.2)	524.6(74.4)
38	151.6(18.3)	84.0(10.1)	8.7(1.1)	74.6(23.4)	116.4(21.6)	513.8(73.4)
40	147.5(17.8)	81.6(9.8)	9.2(1.1)	80.9(25.0)	121.9(22.1)	493.8(71.8)

TABLE III. Experimental Production and Ionization cross sections of Pb.

Energy (KeV)	Production cross section			Ionization cross section		
	L_α (barn)	L_β (barn)	L_γ (barn)	L_1 (barn)	L_2 (barn)	L_3 (barn)
20	20.5(2.0)	02.8(0.3)	064.6(8.0)
22.5	46.8(5.6)	10.3(1.0)	147.5(18.4)
25	68.2(8.1)	21.9(2.0)	2.1(0.3)	..	19.8(3.2)	213.0(26.8)
27.5	87.6(10.5)	31.5(3.1)	5.6(0.7)	29.2(7.3)	41.6(7.1)	252.2(34.7)
30	103.8(12.5)	44.6(3.9)	6.2(0.8)	32.0(8.0)	46.5(7.9)	301.1(41.1)
32.5	113.4(13.6)	51.7(4.5)	6.9(0.8)	33.9(8.4)	52.3(8.9)	329.2(44.8)
35	114.9(13.8)	53.9(4.7)	7.7(0.9)	36.8(9.3)	58.0(9.8)	331.7(45.5)
37.5	122.1(14.6)	56.7(5.0)	8.0(1.0)	36.5(9.1)	61.6(10.4)	354.0(48.3)
40	129.5(15.5)	62.6(5.4)	8.9(1.1)	39.8(10.1)	68.9(11.6)	374.5(51.3)
42.5	124.9(15.0)	59.8(5.3)	9.5(1.2)	41.0(10.3)	74.0(12.4)	358.5(49.5)
45	127.9(15.3)	62.9(5.5)	8.9(1.1)	42.1(10.4)	68.0(11.6)	368.0(50.6)

TABLE IV. Experimental Production and Ionization cross sections of Th.

lating the ionization cross sections for electron or positron impact is given by Bote et. al. [13]. The details of the MRBEB theory involved in these estimates can be found in Ref. [10–12]. The theoretical L -shell ionization cross sections, obtained from these formalisms, are converted into production cross sections using Eqs. 5, 8, and 9 along with the relevant relaxation parameters [17].

$$\sigma_{L_\beta} = \sigma_{L_1}[\omega_1 S_{\beta,1} + \omega_2 f_{12} S_{\beta,2} + \omega_3 (f_{13} + f_{12} f_{23}) S_{\beta,3}] + \sigma_{L_2}(\omega_2 S_{\beta,2} + \omega_3 f_{23} S_{\beta,3}) + \sigma_{L_3} \omega_3 S_{\beta,3} \quad (8)$$

$$\sigma_{L_\gamma} = \sigma_{L_1}[\omega_1 S_{\gamma,1} + \omega_2 f_{12} S_{\gamma,2}] + \sigma_{L_2} \omega_2 S_{\gamma,2} \quad (9)$$

While comparing with theory, it should be noted that the relaxation parameters, which are used to obtain theoretical production cross sections, can themselves have uncertainties $\lesssim 50\%$. Table V shows the recommended uncertainties in Ref.[15], which are adopted in this work.

Parameters	ω_1	ω_2	ω_3	f_{12}	f_{13}	f_{23}	Γ, s
% Error	20	5	5	50	15	10	10

TABLE V. Adopted errors in relaxation parameters.

The L X-ray production cross sections of Lead and Thorium are plotted in the Figures 4 and 5 respectively. Corresponding theoretical estimates, based on the DWBA and the MRBEB theories are also plotted on the same graphs. The shaded regions around the DWBA estimates in both the graphs indicate the predicted uncertainty bands arising from the uncertainties in the adopted relaxation parameters.

In case of Lead, the L_α and L_β X-ray production cross sections, based on measurements done by Wu et al.[18] and Moy et al.[19], are also shown in the Fig. 4. These two sets of measurements are in good agreement with

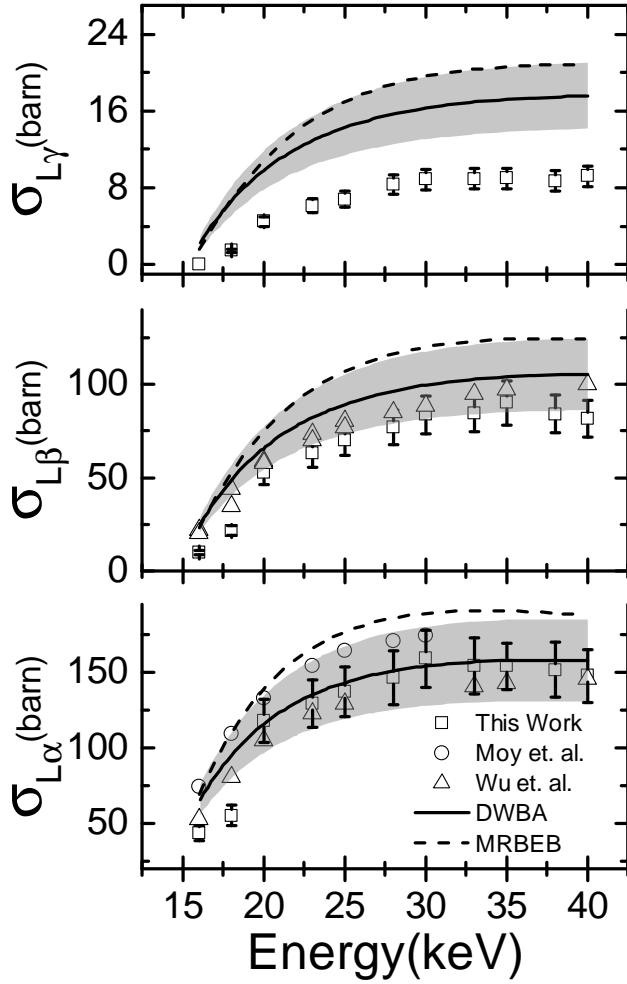


FIG. 4. Production cross section of L_α , L_β and L_γ lines of Pb. Theoretical curves are obtained using relaxation parameters from [15] and [16]. The shaded area is due to the uncertainty in the adopted relaxation parameters.

our corresponding results. The DWBA estimates for the L_α production cross sections of both the elements are in good agreement with all three experimental data sets. The DWBA estimates for L_β lines of Lead overpredict the production cross sections across the energy range of interest, but the estimates agree with the experimental results within the predicted uncertainty band. Considering the systematic trend in the experimental data over the energy range, the results of Wu et al.[18] are in better agreement within the uncertainty band. Our results for Lead are systematically on the lower end of the predicted band. The MRBEB theory predicts larger production cross sections in all the cases, with values grazing the upper end of the predicted uncertainty band of DWBA estimates.

No other measurement of the L X-ray production cross sections of Thorium exists to the best of our knowledge. Our results agree with the DWBA estimates for the L_α line (see Fig. 5). Comparison with DWBA estimates for

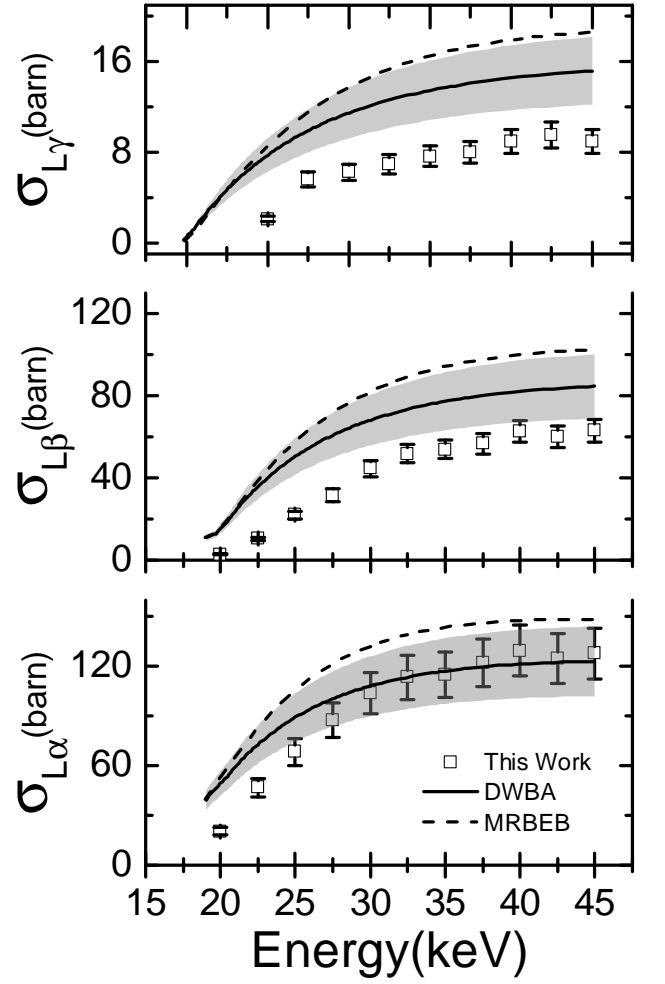


FIG. 5. Production cross section of L_α , L_β and L_γ lines of Th. Theoretical curves are obtained using relaxation parameters from [15] and [16]. The shaded area is due to the uncertainty in the adopted relaxation parameters.

the L_β and L_γ production cross sections of Thorium indicate the similar trend as that in Lead.

The discrepancy between theory and experiment can be further understood by looking at the L_1 , L_2 , and L_3 ionization cross sections extracted from our experimental data. The ionization cross sections obtained from our experiment, along with theoretical estimates, are plotted in the Figs. 6 and 7 for Lead and Thorium respectively. In both the elements, the L_3 ionization cross section is explained very well by the DWBA theory, specifically for the energies $E > 1.35U$, where U is the ionization threshold for the L_3 subshell. Also it is important to note that the L_3 subshell ionization cross sections for only a handful of elements in the range from Phosphorus ($Z = 15$) to Uranium ($Z = 92$), measured either directly from electron energy loss spectroscopy (EELS) or indirectly by electron impact spanning energy range from near the ionization threshold to ~ 1 MeV, are found to agree reasonably well with the DWBA calculations following Bote

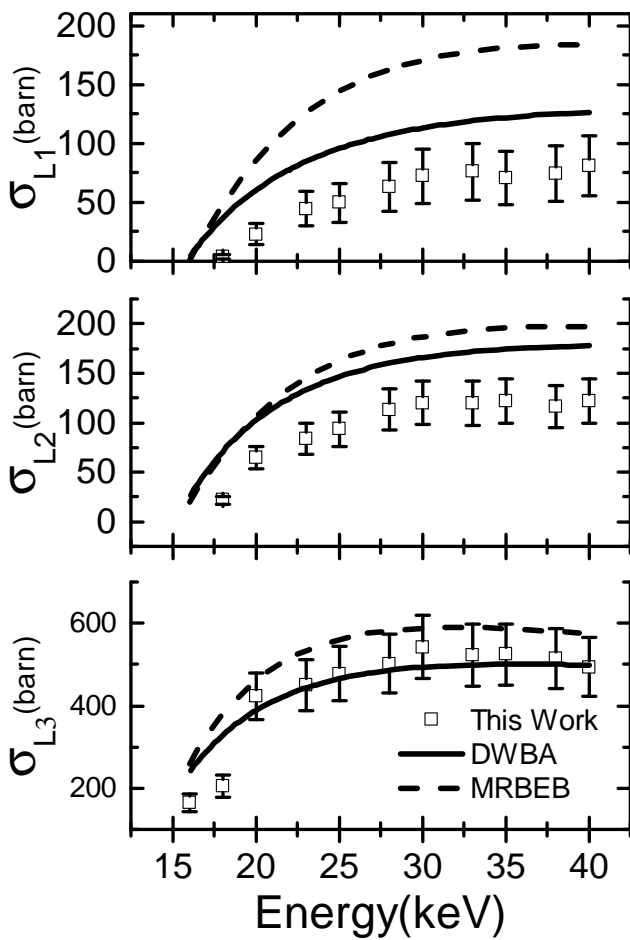


FIG. 6. L_1 , L_2 and L_3 subshell ionization cross sections of Lead.

et al.[8], as described in detail in Ref. [20]. The agreement is very limited especially at energies near the ionization threshold. But in case of L_2 and L_1 subshells, the agreement between theory and experiment is not at all satisfactory. In both the elements studied in our experiment, the L_2 and L_1 subshell ionization cross sections at near-threshold energies are smaller than the DWBA estimates by $\sim 30 - 50\%$. The MRBEB theory predicts $\sim 20 - 30\%$ higher ionization cross sections than the DWBA theory for L_2 and L_3 subshells and up to 80% higher for L_1 subshell.

The difference in theory and experiment for L_1 and L_2 sub-shell results can be due to the relaxation parameters used in the estimation of these ionization cross sections. A direct indication of the results of relaxation parameter variation is given in Sec. III in connection with our attempt in extracting σ_{L_1} and σ_{L_2} for Thorium from the corresponding σ_{L_α} and σ_{L_γ} . While calculating the σ_{L_1} from the corresponding $\sigma_{L_{\gamma_{236}}}$ for both the elements, we have used the radiative yields $\Gamma_{\gamma_1}, \Gamma_{\gamma_6}, \Gamma_{\gamma_2}, \Gamma_{\gamma_3}$ and the fluorescence yield (ω_1). Out of these five relaxation parameters, $\Gamma_{\gamma_2}, \Gamma_{\gamma_3}$ and ω_1 are associated with the relaxation of the vacancy created in the L_1 subshell, and the

remaining parameters are associated with the vacancy in the L_2 subshell. Thus, our experimental findings indicate that the differences between theory and experiment could be due to the poorly known relaxation parameters, specifically the relaxation parameters related to the L_1 subshell. It is worth mentioning here that in a review on theories of inner shell ionization by proton impact[21], the author has concluded that the radiative yield related to the L_1 subshell and the Coster- Kronig factors need to be re-evaluated and experimentally measured.

The L_2 subshell results are inconclusive due to the fact that the σ_{L_2} , obtained from $\sigma_{L_{\gamma_{1+5}}}$ is lower than the theoretical estimates by $30 - 50\%$, but the σ_{L_β} values, which have almost equal contribution from σ_{L_2} and σ_{L_3} , are explained reasonably well by the DWBA theory, specifically for Lead and other high Z elements[7, 12]. The σ_{L_3} and σ_{L_α} results are explained very well by theory, not only for the Pb and Th, but also for the other high Z elements[7, 12], indicating that the relaxation parameters related to L_3 subshell are consistent with the underlying theory and related experiments.

From our study, it is evident that the discrepancy between theory and experiment may arise due to errors in fixing some of the relaxation parameters. It is, therefore, important to perform measurements, which require a minimum number of relaxation parameters for extracting ionization cross sections from the experimental data. Clearly, more measurements with wavelength dispersive spectrometer should be done where resolution is so high that even a single transition can be studied, thereby reducing the dependence on the relaxation parameters. Also, very few measurements exist for the L_γ X-ray production cross sections of high Z elements. As L_γ transitions relate to the L_1 and L_2 subshells, it is important to perform these measurements, specifically in view of the new calculations performed by Pindzola [4, 22] by the inclusion of the retarded electromagnetic potential, which significantly changes the ionization cross sections of the L_1 and L_2 subshells.

V. CONCLUSION

We have obtained the subshell resolved ionization cross sections from the production cross sections involving the L -shell in Lead and Thorium. Results are compared with two different theoretical formalisms *viz.*, MRBEB and DWBA. The experimental results are reproduced reasonably well by the DWBA theory for the L_3 subshell and the L_α transition, but poor agreement is found for L_1 and L_2 subshells and consequently for the L_β and the L_γ transitions in both the elements. MRBEB theory overpredicts the cross sections for all the three subshells in both the elements in the electron impact energy regime explored in our experiment. Discrepancy between DWBA theory and our experiment points to the poor knowledge of the relaxation parameters related to the L_1 subshell. From our study, we conclude that more

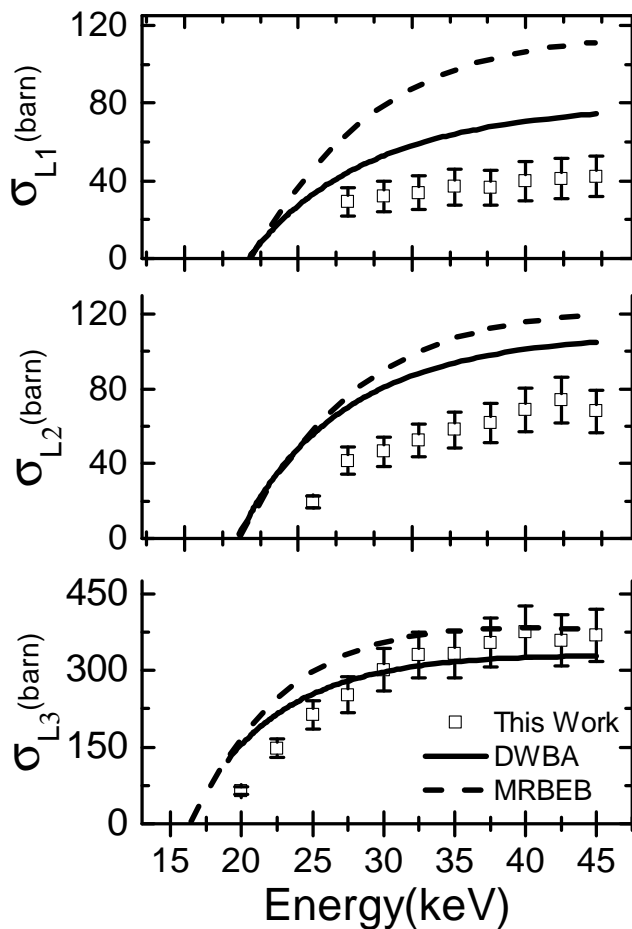


FIG. 7. L_1 , L_2 and L_3 subshell ionization cross sections of Thorium.

precise measurements of the corresponding sub-shell resolved cross sections are urgently needed to obtain the relaxation parameters with better precision.

ACKNOWLEDGMENTS

This research work is supported by grant no. 12-R&D-SIN-5.02-0102 of the Department of Atomic Energy, Government of India. Two of the authors (M.G. and J.P.S.) would like to acknowledge research support in part by Fundação Fundacao para a Ciência e Tecnologia (FCT), Portugal, through the Project No. PEstOE/FIS/UI0303/2011 financed by the European Community Fund FEDER through the COMPETE. M. G. also acknowledges the support of the FCT, under Contract No. SFRH/BPD/92455/2013. The authors acknowledge the fabrication of the experimental setup by the SINP machine shop.

-
- [1] C. J. Powell, *Rev. Mod. Phys.* **48**, 33 (1976).
[2] W. Bambynek, B. Crasemann, R. W. Fink, H. U. Freund, H. Mark, C. D. Swift, R. E. Price, and P. V. Rao, *Rev. Mod. Phys.* **44**, 716 (1972).
[3] D. Chattarji, *The Theory of Auger Transitions* (Elsevier Science, 1976).
[4] M. S. Pindzola, *Journal of Physics B: Atomic, Molecular and Optical Physics* **48**, 015201 (2015).
[5] D. C. Joy, *Scanning* **17**, 270 (1995).
[6] Y. Wu, Z. An, Y. M. Duan, and M. T. Liu, *Journal of Physics B: Atomic, Molecular and Optical Physics* **43**, 135206 (2010).
[7] J. M. Fernández-Varea, S. Segui, and M. Dingfelder, *Phys. Rev. A* **83**, 022702 (2011).
[8] D. Bote and F. Salvat, *Phys. Rev. A* **77**, 042701 (2008).
[9] J. M. Fernández-Varea, F. Salvat, and J. Sempau, "Penelope 2011: a code system for monte carlo electron and photon transport, nea data bank, nea/nsc/doc(2011)5,".
[10] M. Guerra, F. Parente, P. Indelicato, and J. Santos, *International Journal of Mass Spectrometry* **313**, 1 (2012).
[11] M. Guerra, P. Amaro, J. Machado, and J. P. Santos, *Journal of Physics B: Atomic, Molecular and Optical Physics* **48**, 185202 (2015).
[12] H. V. Rahangdale, M. Guerra, P. K. Das, S. De, J. P. Santos, D. Mitra, and S. Saha, *Phys. Rev. A* **89**, 052708 (2014).
[13] D. Bote, F. Salvat, A. Jablonski, and C. J. Powell, *Atomic Data and Nuclear Data Tables* **95**, 871 (2009).
[14] G. Lapicki, A. Mandal, S. Santra, D. Mitra, M. Sarkar, D. Bhattacharya, P. Sen, L. Sarkadi, and D. Trautmann, *Physical Review A* **72**, 022729 (2005).
[15] J. Campbell, *Atomic Data and Nuclear Data Tables* **85**, 291 (2003).
[16] J. Campbell and J.-X. Wang, *Atomic Data and Nuclear Data Tables* **43**, 281 (1989).
[17] K. Shima, T. Nakagawa, K. Umetani, and T. Mikumo, *Phys. Rev. A* **24**, 72 (1981).
[18] Y. Wu, Z. An, Y. M. Duan, M. T. Liu, and C. H. Tang, *Journal of Physics B: Atomic, Molecular and Optical Physics* **40**, 735 (2007).
[19] A. Moy, C. Merlet, X. Llovet, and O. Dugne, *Journal of Physics B: Atomic, Molecular and Optical Physics* **46**, 115202 (2013).
[20] X. Llovet, C. J. Powell, F. Salvat, and A. Jablonski, *Journal of Physical and Chemical Reference Data* **43**, 013102 (2014).

- [21] J. Miranda, C. Romo-Kröger, and M. Lugo-Licona, Nuclear Instruments and Methods in Physics Research, Section B: Beam Interactions with Materials and Atoms **189**, 21 (2002).
- [22] M. S. Pindzola, Physical Review A **90**, 13 (2014).